Gravity anomalies, crustal structure and thermo-mechanical support of the Himalaya of Central Nepal

R. Cattin, G. Martelet, P. Henry, J. P. Avouac, M. Diament, T. R. Shakya

Geophys. J. Int. (2001) **147,** 381–392

Gravity anomalies, crustal structure and thermo-mechanical support of the Himalaya of Central Nepal

R. Cattin,[1] G. Martelet,[2] P. Henry,[1] J. P. Avouac,[1,3] M. Diament[2] and T. R. Shakya[4]

[1] *Laboratoire de Géologie, ENS Paris,* 24 *rue Lhomond,* 75231 *Paris, France. E-mail: cattin@mailhost.geologie.ens.fr*
[2] *Laboratoire de Gravimétrie et Géodynamique,* UMR 7577, *IPGP,* 4 *place Jussieu,* 75252 *Paris, France*
[3] *Laboratoire de Détection et de Géophysique, CEA,* B.P. 12, 91680, *Bruyères-le-Châtel, France*
[4] *PEPP, Department of Mines and Geology, Lainchaur, Kathmandu, Nepal*

Accepted 2001 June 8. Received 2001 January 6; in original form 2000 February 4

SUMMARY

We use two gravity profiles that we measured across Central Nepal, in conjunction with existing data, to constrain the mechanical behaviour and the petrological structure of the lithosphere in the Himalayan collision zone. The data show (1) overcompensation of the foreland and undercompensation of the Higher Himalaya, as expected from the flexural support of the range; (2) a steep gravity gradient of the order of 1.3 mgal km^{-1} beneath the Higher Himalaya, suggesting a locally steeper Moho; and (3) a 10 km wide hinge in southern Tibet. We compare these data with a 2-D mechanical model in which the Indian lithosphere is flexed down by the advancing front of the range and sedimentation in the foreland. The model assumes brittle Coulomb failure and non-linear ductile flow that depends on local temperature, which is computed from a steady-state thermal model. The computed Moho fits seismological constraints and is consistent with the main trends in the observed Bouguer anomaly. It predicts an equivalent elastic thickness of 40–50 km in the foreland. The flexural rigidity decreases northwards due to thermal and flexural weakening, resulting in a steeper Moho dip beneath the high range. Residuals at short wavelengths (over distances of 20–30 km) are interpreted in terms of (1) sediment compaction in the foreland ($\Delta\rho = 150$ kg m^{-3} between the Lower and Middle Siwaliks); (2) the contact between the Tertiary molasse and the meta-sediments of the Lesser Himalaya at the MBT ($\Delta\rho = 220$ kg m^{-3}); and (3) the Palung granite intrusion in the Lesser Himalaya ($\Delta\rho = 80$ kg m^{-3}). Finally, if petrological transformations expected from the local (P, T) are assumed, a gravity signature of the order of 250 mgal is predicted north of the Lesser Himalaya, essentially due to eclogitization of the lower crust, which is inconsistent with the gravity data. We conclude that eclogitization of the Indian crust does not take place as expected from a steady-state local equilibrium assumption. We show, however, that eclogitization might actually occur beneath southern Tibet, where it could explain the hinge observed in the gravity data. We suspect that these eclogites are subducted with the Indian lithosphere.

Key words: eclogitization, gravity anomaly, Himalaya, layered rheology, mechanical modelling, thermal modelling.

1 INTRODUCTION

The structure of the lithosphere across the Himalaya of Nepal (Fig. 1) has been investigated through a variety of means, including gravity and seismic techniques (e.g. Lyon-Caen & Molnar 1983, 1985; Hirn *et al.* 1984; Zhao *et al.* 1993). The Indian shield dips gently beneath the overthrusting range, forming a foreland basin filled with Cenozoic molasse (Fig. 2a). The molasse are scraped from the basement along the Main Himalayan Thrust fault, MHT, and form an active fold belt along the Himalayan foothills (Lavé & Avouac 2000). The MHT flattens beneath the Lesser Himalaya and roots deeper beneath the Higher Himalaya and southern Tibet. The Bouguer anomaly in India and in Tibet primarily indicates local Airy compensation (e.g. Lyon-Caen & Molnar 1983, 1985; Jin *et al.* 1994, 1996) (Fig. 2b). By contrast, the gravity measurements across the Himalaya show important deviations from Airy isostasy (Fig. 2b), suggesting that the weight of the Himalaya is

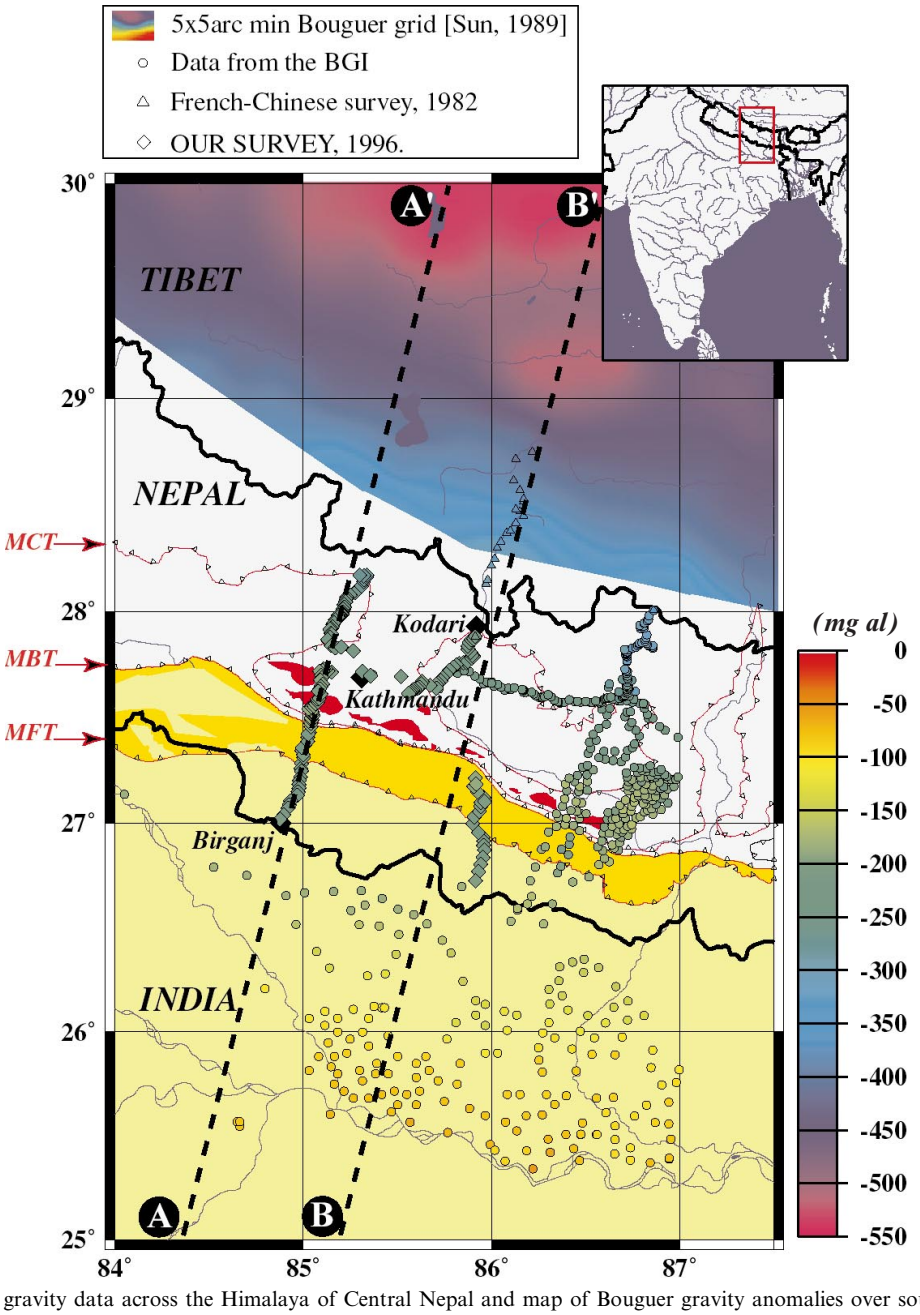

Figure 1. Location of gravity data across the Himalaya of Central Nepal and map of Bouguer gravity anomalies over southern Tibet from Sun (1989). The colour scale shows complete Bouguer anomalies. Also shown are Palung granites (red), Siwaliks units (orange) and Quaternary deposits in the foreland (yellow). Black dashed lines show the locations of profiles AA′ and BB′.

supported by the strength of the underthrusting Indian plate. Flexural modelling in terms of a thin elastic plate overlying an inviscid fluid successfully reproduces these deviations but requires that some additional forces contribute to support the high topography (Lyon-Caen & Molnar 1983, 1985; Jin *et al.* 1996). It has also been inferred that some amount of low-density molasse has been thrust beneath the range and that the strength of the Indian plate must decrease abruptly to account for the steep gravity gradient beneath the Higher Himalaya (Lyon-Caen & Molnar 1983).

In this paper we examine the gravity data in order to address more particularly two issues. One is that the density of the Himalayan crust might not be uniform due to the thermal structure and possible petrological changes related to the underthrusting of the Indian crust (Le Pichon *et al.* 1997; Henry *et al.* 1997). These effects may indeed have a large gravity signature and should therefore be considered. The second is that modelling of the flexural support of the range taking account of a realistic rheology (e.g. Burov & Diament 1995, 1996) may lead to a different appreciation of the force balance than previous analyses based on thin elastic plates that cannot account for weakening during flexural straining (Ranalli 1994; Burov & Diament 1995) or thermal weakening (Cattin & Avouac 2000). We therefore based our analysis on a mechanical model with a realistic temperature- and pressure-dependent rheology.

Since most of the deviation from local isostatic compensation occurs across the Himalaya, where lateral rigidity variations as well as structural and thermal effects might be suspected, there

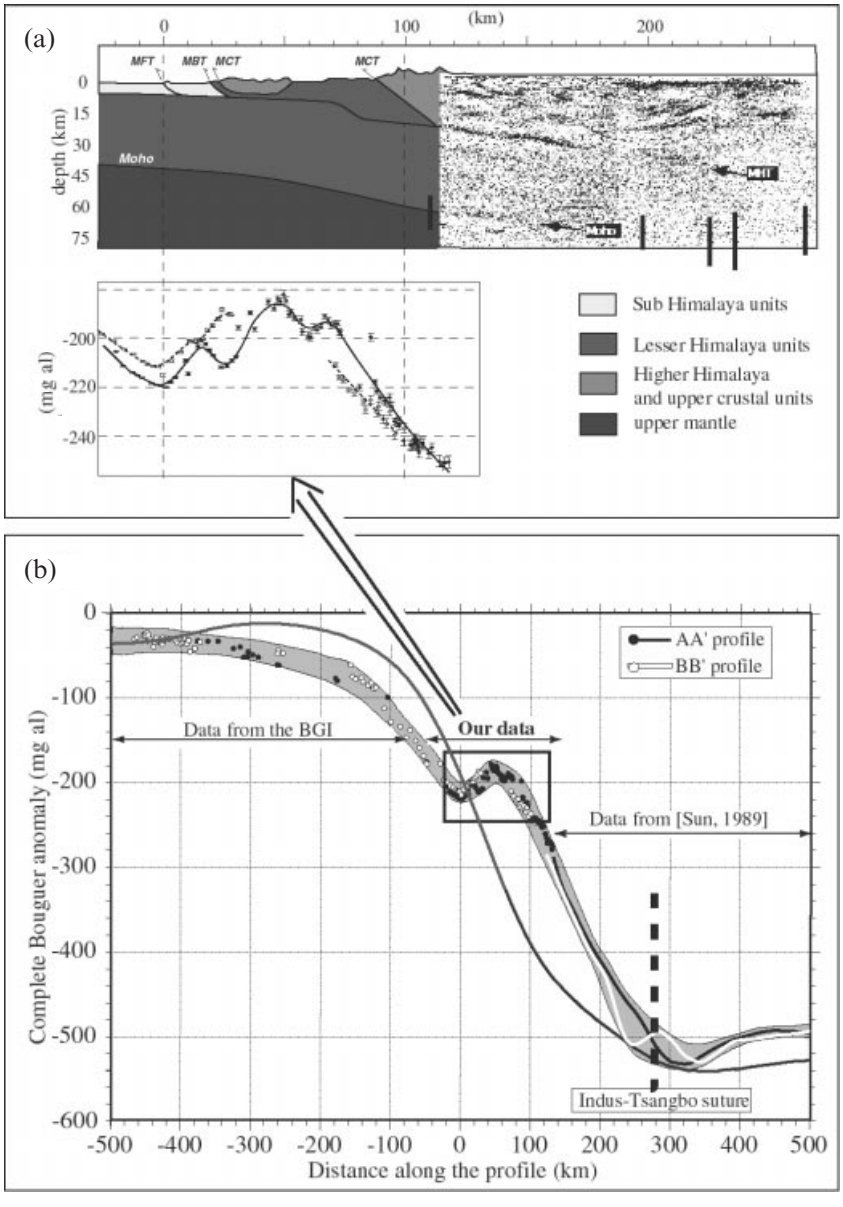

Figure 2. (a) Simplified structural N18°E section along profile AA′ across the Himalaya of Central Nepal. Cenozoic molasse in the foreland, metasediments in the Lesser Himalaya, and crystalline units in the High Himalaya are distinguished. The geometry of the MHT includes a subhorizontal plane beneath the Lesser Himalaya and a mid-crustal ramp beneath the Higher Himalaya (from Lavé & Avouac 2000). The Moho is set to 40 km beneath the Indian shield according to teleseismic receiver functions (Saul *et al.* 2000). INDEPTH seismic profiles (Zhao *et al.* 1993; Brown *et al.* 1996), and Moho picks on receiver functions (Kind *et al.* 1996), thick vertical bars, are also reported. (b) Complete Bouguer anomaly along profiles AA′ and BB′ (see Fig. 1 for locations of profiles). All the data within a 30 km wide swath centred on each profile were considered. Light-grey shading shows the 2-D gravity profile taking account of lateral variations in the study area. The black solid line shows the Bouguer anomalies expected from Airy local isostasy. the inset shows a close-up view of the data acquired across Nepal in this study. $x = 0$ corresponds to the location of the Main Frontal Thrust fault, MFT, where the MHT reaches the surface at the front of the sub-Himalaya.

was a need for accurate gravity data in this area. The available data (Kono 1974; Das *et al.* 1979; Lyon-Caen & Molnar 1983, 1985) are sparse, have large uncertainties of the order of 15–30 mgal, and are sometimes affected by flaws (Jin *et al.* 1996). For the purpose of this study, in 1996 we carried out a detailed gravity survey along two profiles that cross the range near the Kathmandu basin (Fig. 1).

Hereafter, (1) we present these new gravity data and combine them with pre-existing data from Tibet (Sun 1989) and India (data from the Bureau Gravimétrique International); (2) we compare them with calculated gravity anomalies associated with Moho geometry computed from a mechanical model based on a temperature- and pressure-dependent rheology; (3) we analyse short-wavelength residuals and their correlation with upper crustal structures; and finally (4) we discuss the density contrasts, and their gravity signature, that might be expected from the (P, T) conditions at depth.

2 DATA

Gravity measurements were carried out at 152 sites along two profiles perpendicular to the Himalaya at the longitude of

Kathmandu (see diamonds in Fig. 1). The data were acquired using two Scintrex CG3 and CG3-M meters that had previously been intercalibrated. The whole data set has been tied to the IGSN 71 network in Kathmandu airport base. The vertical positions of the stations were obtained from the Nepalese Geodetic Survey benchmarks or using differential GPS. The vertical accuracy of the positioning is better than 1 m. Horizontal x and y coordinates were determined using GPS in mono-receptor mode, with an estimated accuracy of better than 100 m. The free-air anomaly was computed using the GRS 67 ellipsoid. Combining the gravity values measured with both instruments, we estimate the overall accuracy of the free-air anomaly to be of the order of 0.2 mgal. For consistency with the gridded Bouguer anomaly over China (Sun 1989), the complete Bouguer anomaly is computed using a reference density of 2670 kg m^{-3}. Inner zone terrain corrections B and C were estimated in the field using Hammer charts. Outer zones, up to 167 km, were computed with 20 m $\times$ 20 m and 1 km $\times$ 1 km digital elevation models using GRAVSOFT package software (Forsberg 1985). The resulting complete Bouguer anomaly has an accuracy ranging from 0.5 to 5 mgal, depending on the terrain roughness.

In order to construct continuous profiles from India to Tibet, we merged several gravity data sets (Fig. 1). To the south of Nepal, in India, the data come from the Bureau Gravimétrique International database (BGI, Toulouse, France; http://www-projet.cnes.fr). These data are tied to the IGSN 71 network and do not include terrain corrections. Their accuracy is about 1 mgal. To the north of Nepal, data come both from a French–Chinese profile (Abtout 1987) and from gridded Bouguer anomalies (Sun 1989). The French–Chinese data were measured in 1982 (Van de Meulebrouck 1983) in the southern part of Tibet. They include terrain corrections computed up to 22 km. Originally, these data were tied to the Postdam gravity reference. Following Woollard & Godley (1980), we converted them to IGSN 71. Van de Meulebrouck (1983) estimates their accuracy to be between 3 and 7 mgal. The 5 arcmin $\times$ 5 arcmin gridded complete Bouguer anomalies over China were reduced using Helmert normal gravity formulae and tied to the Postdam standard (Sun 1989). They comprise terrain corrections computed up to 167 km. Since we do not have the raw data, we could not convert the grid to the IGSN 71/GRS 67 standard. This would have induced shifts of less than 8 mgal. The error on the original grid itself is estimated to be 1.5 mgal (Sun 1989). Finally, where this was necessary, we recomputed the terrain corrections up to 167 km in order to obtain a data set as homogeneous as possible.

Two 1000 km long, N18°E profiles (AA′ and BB′) were obtained by projecting all the data located within 15 km wide swaths (Fig. 2). The two profiles are quite similar: the Bouguer anomaly decreases from south to north, from about -40 to -500 mgal, and exhibits a steep gradient beneath the high range as observed along other profiles across the Himalaya. Locally (around $x = 0$ km on Fig. 2b), the data also exhibit a stair-shaped geometry that can be associated with the sediments accumulated in the foreland basin (e.g. Lyon-Caen & Molnar 1983, 1985). There are small variations between the profiles, with amplitudes of the order of less than 10 mgal and wavelengths of a few tens of kilometres at most, that reflect lateral geological changes in the upper crust. To first order, the gravity data thus reflect an essentially 2-D geometry that can be represented by the shaded area shown in Fig. 2(b). This envelope accounts for uncertainties on gravity data as well as for the differences between the AA′ and BB′ profiles. In the following, we consider this profile to be representative of the average 2-D gravity response of the Himalaya of Central Nepal (Fig. 2b).

3 FLEXURAL SUPPORT OF THE HIMALAYA

3.1 Discrepancy between the observations and Airy model

Local Airy isostasy is verified at distance from the range, so some estimate of the density contrast at the Moho can be inferred from the variation of crustal thickness. Teleseismic receiver functions suggest that the crust is 35–40 km thick beneath India, south of the Gangetic foreland (Saul *et al.* 2000). A crustal thickness of 70–75 km was estimated beneath Tibet from the INDEPTH seismic experiment (e.g. Zhao *et al.* 1993; Brown *et al.* 1996). This difference of crustal thickness and the 460 mgal difference of Bouguer anomalies between India and Tibet suggest a density contrast between the crust and upper mantle of 370 kg m^{-3}, consistent with the findings of Jin *et al.* (1996). If we now compare the measured profile with that predicted from local Airy isostasy, computed for this density contrast at the Moho, we find significant departures from local isostasy (Fig. 2b). The foreland appears overcompensated while the high range is undercompensated. These are clear manifestations of a regional flexural support of the Himalayan topography (e.g. Kono 1974; Lyon-Caen & Molnar 1983, 1985).

3.2 Description of the mechanical model and thermal structure

In order to model the mechanical support of the range, we use the 2-D finite element model ADELI (Hassani *et al.* 1997). The model was modified to account for the non-Newtonian rheology of the lithosphere and its dependence on temperature and pressure (Cattin & Avouac 2000). We assume a constant density contrast of 370 kg m^{-3} between the crust and the mantle, and of 300 kg m^{-3} between the sediments accumulated in the foreland basin and the underlying Indian crust. As an initial condition, the Indian crust is flat and its thickness is supposed to be 40 km (Fig. 3). The model is submitted to gravitational forces ($g = 9.81$ ms^{-2}) and is supported at its base by hydrostatic pressure. We allow for free vertical displacements at both ends of the model.

As argued by Nelson *et al.* (1996), we consider an Indian mantle lid that underthrusts the Himalaya and southern Tibet. The long-term horizontal convergence between India and southern Tibet is estimated to be 21.0 ± 1.5 mm yr^{-1} (Lavé & Avouac 2000). It is accommodated by slip along the Main Himalayan Thrust fault that marks the limit between the Indian plate and the overthrusting Himalayan and Tibetan crust. Because the Himalaya are submitted to intense erosion, which removes about 300 km^3 km^{-1} Myr^{-1}, the edge of the overriding plate proceeds more slowly at 10–15 mm yr^{-1}. We therefore model the collision between India and Asia by gradually loading the Indian plate by the Himalayan topography with a convergence rate of 15 mm yr^{-1} (Fig. 3).

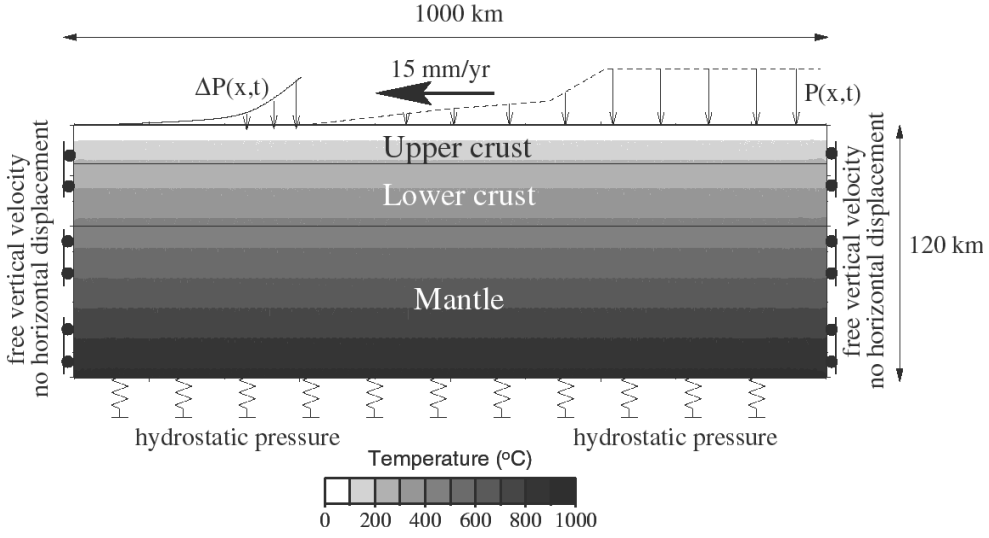

Figure 3. Geometry and boundary conditions used for mechanical modelling. The initially flat Indian lithosphere is progressively loaded $P(x, t)$ by the Himalayan front which is assumed to advance at a rate of 15 mm yr^{-1}. This rate was deduced from the $\sim$20 mm yr^{-1} rate of thrusting corrected for a $\sim$5 mm yr^{-1} parallel retreat term due to erosion. The basal boundary condition is hydrostatic allowing for isostatic balance. Sedimentation in the Ganga plain is assumed to maintain a flat foreland at a constant elevation (arbitrarily fixed to 0 m), inducing an additional load $\Delta P(x, t)$. The sediment overburden is computed assuming a sediment density of 2400 kg m^{-3}. The upper crust, lower crust and upper mantle have different rheologies, as described in Table 1.

Sedimentation is assumed to maintain a flat foreland at a constant elevation south of the MFT. It implies that, in the foreland, sedimentation balances flexural subsidence. We model the filling of the flexural basin by increasing the subsurface load by

$$\Delta P = \rho_s g h_{sub} \tag{1}$$

at each time step, where ρ_s is the density of sediment, g the gravity acceleration, and h_{sub} the subsidence of the Indian plate in the foreland.

The model accounts for the variation of rheology with depth in the lithosphere (see parameters in Table 1). We consider an upper crust with a quartz-like rheology and a lower crust with either a diabase- or a quartz-like rheology. An olivine ductile flow law is assumed for the upper mantle. Rocks deform elastically, brittlely or ductilely depending on the local deviatoric stresses, pressure and temperature. Elastic deformation is defined by the relationship between strain (ε_{ij}) and stress (σ_{ij}):

$$\varepsilon_{ij} = \frac{1+\nu}{E}\,\sigma_{ij} - \frac{\nu}{E}\,\sigma_{kk}\delta_{ij}\,, \tag{2}$$

where E and ν are Young's modulus and Poisson's ratio, respectively. Beyond the elastic domain, we use an elasto-plastic pressure-dependent law with a Drucker–Prager failure criterion:

$$\frac{1}{2}\,(\sigma_1 - \sigma_3) = \left[c(\cot\phi) + \frac{1}{2}\,(\sigma_1 - \sigma_3)\right]\sin\phi\,, \tag{3}$$

where c is the cohesion and ϕ is the internal friction angle.

Ductile flow is described as a power-law creep (Carter & Tsenn 1987; Tsenn & Carter 1987; Kirby & Kronenberg 1987):

$$\dot{\varepsilon} = \gamma_0(\sigma_1 - \sigma_3)^n \exp(-E_a/RT)\,, \tag{4}$$

where R is the universal gas constant, T the temperature, E_a the activation energy, and γ_0 and n are empirically determined constants, assumed not to vary with stress and (P, T) conditions.

We assume a steady-state thermal structure computed from the 1-D approximation of Royden (1993), with parameters taken from Henry *et al.* (1997) (Fig. 4b). We impose a temperature of 0 °C at the Earth surface and a constant mantle heat flow of 15 mW m^{-2} at the base of the model. The upper crust heat production is taken to be 2.5 μW m^{-3}. This thermal structure is consistent with the characteristics of metamorphic rocks exhumed from the Himalaya (Royden 1993; Henry *et al.* 1997). The computed thermal structure of the Indian plate, away from the Himalaya, implies a surface heat flow of about 60 mW m^{-2}, consistent with the measurements made in cratonic areas of northern India (Pandey *et al.* 1999).

In all experiments we obtain a nearly steady-state Moho that migrates southwards with respect to fixed India. Hereafter we will consider the geometry obtained after 10 Myr, which is nearly steady-state.

Table 1. Physical parameters and material properties used for the mechanical modelling: ρ, density; E, Young's modulus; ν, Poisson's ratio; c, cohesion; ϕ, internal friction angle; γ_0, power-law strain rate, n power-law exponent, and E_a power-law activation energy.

	Quartz (upper crust)	Diabase (lower crust)	Olivine (upper mantle)
ρ (kg/m^{-3})	2900	2900	3270
E (GPa)	80	80	80
ν	0.25	0.25	0.25
c (MPa)	10	10	10
ϕ	30°	30°	30°
γ_0 ($Pa^{-n}.s^{-1}$)	6.31×10^{-25}	6.31×10^{-20}	7×10^{-14}
n	2.9	3.05	3
E_a (kJ.mol^{-1})	149	276	510

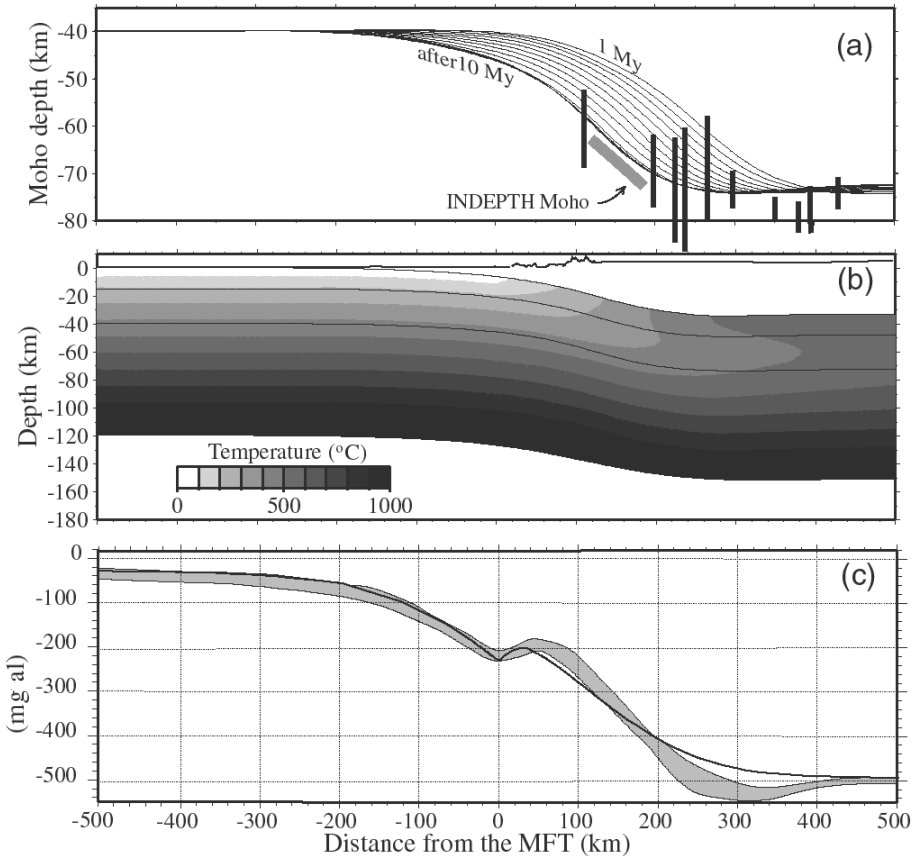

Figure 4. (a) Evolution of the geometry of the Indian Moho during gradual loading. Experiments are run for 10 Myr. The final computed Moho is compared with the Moho determined from the INDEPTH seismic profile (light grey) (Brown *et al.* 1996) or from the receiver functions, vertical bars (Kind *et al.* 1996). (b) Thermal structure of the Indian lithosphere. (c) Bouguer anomaly computed for a density contrast of 370 kg m^{-3} at the Moho and taking account of the low-density sediments in the foreland (density contrast of -300 kg m^{-3} with respect to the upper crust). The model (continuous line) fits the gravity measurements reasonably well.

3.3 Flexural support of the range and estimation of the strength of the lithosphere

In each experiment, the strong Indian plate weakens gradually during its northward course as it is flexed down. The mechanical support of the range results from the elastic cores in the upper crust and upper mantle as well as from shear stresses associated with viscous flow in the lower crust. Since the elastic cores depend on the thermal structure (Fig. 4b), thermal weakening plays an important role, in addition to flexural weakening, in controlling the overall geometry of the system.

The computed Moho geometry for our reference model (Table 1) is in good agreement with the Moho depths and dip as determined from the INDEPTH reflection profiles (e.g. Zhao *et al.* 1993; Brown *et al.* 1996) and receiver functions (Kind *et al.* 1996) (Fig. 4a). The model yields a foreland sedimentary basin that is about 250 km wide and 6 km deep at the MFT. This geometry is consistent with the geometry of the post-orogenic sediment wedge accumulated over the Indian basement, as ascertained from available geological and geophysical data, including well logs, which show on average a 200–300 km width and a 4–5 km maximum depth (Métivier *et al.* 1999).

Assuming a density contrast of 370 kg m^{-3} at the Moho interface and -300 kg m^{-3} between the crust and sediment, we compute the anomaly (Fig. 4c) corresponding to the foreland basin and Moho geometry we obtain after 10 Myr. To first order, the computed anomaly appears in fairly good agreement with the data. In the Ganga basin, the discrepancy between the computed and the measured Bouguer anomaly is less than 25 mgal. Beneath the Higher Himalaya, the gradient of the computed anomaly is of 1.3 mgal km^{-1}, which reflects the 11° northward dip of the computed Moho.

To allow some comparison with thin elastic plate models, our model can be interpreted in terms of the equivalent elastic thickness (EET). The depth-varying rheology leads to the development of decoupled weak layers within the lithosphere (Fig. 5a), responsible for lateral variations of the mechanical rigidity of the lithophere (Burov & Diament 1995). For a plate decoupled into n layers, the equivalent EET, h_{eff}, of the plate is given by (e.g. Burov & Diament 1992)

$$h_{\mathrm{eff}} = \left(\sum_{i=1}^{n} h_i^3 \right)^{1/3}, \qquad (5)$$

where h_i is the elastic thickness of the ith layer. For each layer, we consider the deformation to be elastic when the effective viscosity is greater than 2×10^{25} Pa s; that is, when the relaxation time of the material is twice as long as the time of the experiment (10 Myr).

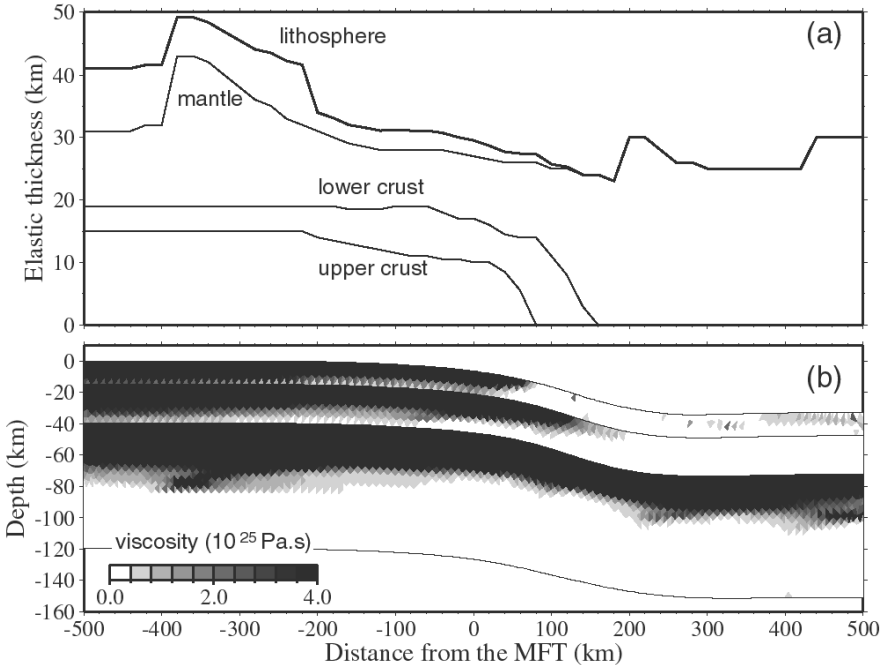

Figure 5. (a) Equivalent elastic thicknesses (EET) of the whole lithosphere and of each of its components (upper /lower crust and mantle). Under the Ganga basin (−500 to −200 km in b), the elastic cores in the upper and lower crust remain coupled assuming a quartz rheology for the upper crust and diabase rheology for the lower crust, but there is some decoupling between the crust and upper mantle. In this case, a 40–50 km EET is obtained, comparable with that estimated by McKenzie *et al.* (1997). An EET as large as 60–70 km under the Gangetic foreland as proposed on the basis of thin elastic plate modelling (e.g. Lyon-Caen & Molnar 1983, 1985) cannot be obtained in our modelling since the crust and the mantle are always partially decoupled. As a result of crustal thickening and temperature increase, decoupling increases northwards. It induces a northward decrease of the EET. This mechanism favours the flexure of the underthrusting Indian lithosphere and leads to a fairly good fit to the gravity data (km −100 to 100 in Fig. 4c).

Even in the relatively cold thermal conditions chosen here [see Henry *et al.* (1997) for an overview], and even assuming a diabase rheology for the lower crust, we observe that coupling between the crust and mantle is never full. The EET is about 40–50 km under the Ganga basin (Fig. 5a), comparable to the value determined by McKenzie & Fairhead 1997). Owing to the quartz-like rheology of the upper crust, decoupling between the upper crust and lower crust develops in response to lithospheric bending. This results in a northward decrease of the EET by about 5 km. We note that our estimates of the EET for the whole lithosphere are lower than those of 60–70 km reported in this area by Lyon-Caen & Molnar (1983, 1985) assuming a Young's modulus $E = 160$ GPa, and than those of 90 km reported by Jin *et al.* (1996). A thicker EET would result in a wider Ganga plain and could improve the fit of the data beyond 200 km. It is unclear, however, whether the presence of a 500 m blanket of sediment as far as 300–400 km away from the Himalayan front is truly attributable to flexural bending or whether it reflects the dynamics of sediment transport. Beneath the Tibetan plateau our estimate for the EET of 30 km is consistent with the value previously proposed by Jin *et al.* (1996).

Still, our modelling fails to reproduce the sharp hinge and gravity upwarp under southern–central Tibet (200–400 km in Fig. 4c). As suggested from previous purely elastic modelling, these features may require a drastic decrease in flexural rigidity across the high range and strong bending moments (Lyon-Caen & Molnar 1983, 1985; Jin *et al.* 1996). We explore another explanation in Section 4.

3.4 Short-wavelength anomalies and density contrasts in the upper crust

As shown in the previous section, the deepening of the Moho beneath the Himalaya, as predicted by our forward model of flexural bending, accounts for the regional trend in the gravity data at long wavelengths (Fig. 4c). There are residuals at short wavelengths that are not negligible, however. South of the Himalayan range, we observe a gravity low of about 100 mgal ($x < 50$ km in Fig. 4c) that has already been noted and ascribed to the sediments accumulated in the foreland (e.g. Lyon-Caen & Molnar 1983). In the light of our new accurate gravity data across Nepal, we can go further and propose some correlation with known geological features such as the MFT, MBT and Palung granites (Fig. 6). We have therefore considered the possibility of density contrasts of lithological origin. Based on a structural section, as defined from balanced cross-sections, and seismic profiles (Schelling & Arita 1991; Lavé & Avouac 2000), we have performed a forward gravity modelling. In the study area, the geometry of the MHT and the location where various structures crop out are well constrained. The MFT (which is the surface trace of the MHT) marks the limit between the undeformed sediments lying on the Indian basement and those that have been scraped off and involved in the Siwalik fold belt. A good fit to the Bouguer anomaly (km −10 to 10 in Fig. 6) is obtained by assuming a density contrast of 150 kg m^{-3} along a 30° to 45° north-dipping interface consistent with the structural dips. It suggests that the Middle and Lower Siwalik molasses

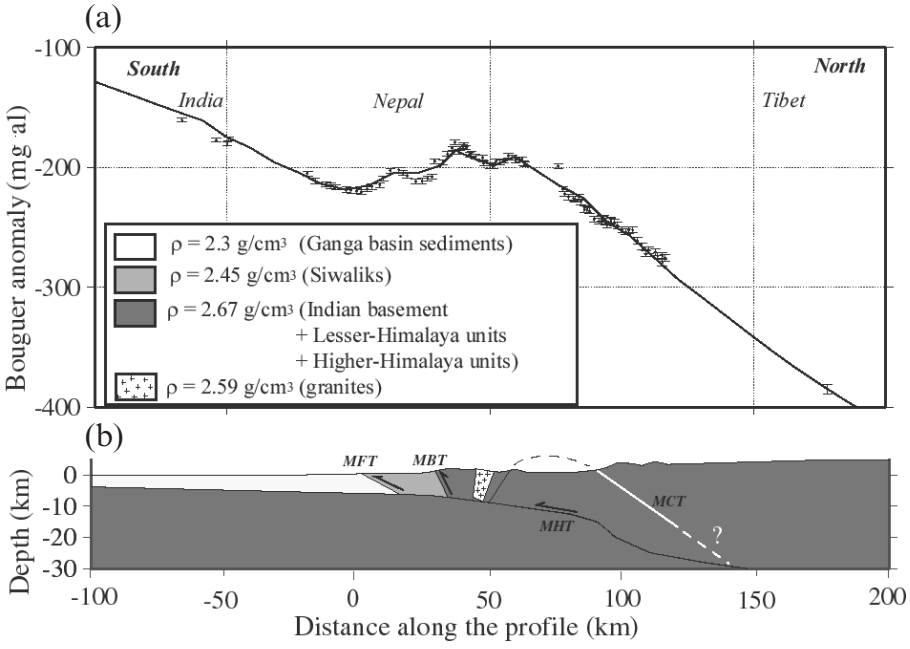

Figure 6. Adjustment of gravity residuals at short wavelengths. (a) Data with error bars. The solid line derives from the density model proposed in (b). (b) The sediments accumulated in the Ganga basin, south of the MFT, are ascribed a density of 2300 kg m^{-3} (e.g. Gansser 1981). Lateral density contrasts of 150 and 220 kg m^{-3} at the MFT and MBT, respectively, are required to fit the data. The Palung granite is assumed to extend to 6 km depth and is ascribed a density of 2600 kg m^{-3}.

which crop out just north of the MFT are more compact than the younger molasse (Upper Siwalik) south of the MFT, probably because they were compacted as a result of the sedimentary overburden of tectonic stresses before being brought up to the surface. At the MBT, a density contrast of 220 kg m^{-3} between the Middle Siwaliks and the meta-sediments in the Lesser Himalaya is inferred from the observed gravity low (km 15 to 35 in Fig. 6). The best-fitting dip of about 60° is in fairly good agreement with structural dips of about 65°. Finally, the gravity low located around $x = 50$ km (Fig. 5) can be correlated with the Palung granite. Wavelet analysis of the Bouguer anomaly (Martelet *et al.* 2001) shows that its vertical extension does not exceed 5–7 km, which corresponds to the base of the hanging wall of the MHT. This is in agreement with MT soundings which also suggest that the Palung granite does not extend deeper than the decollement along the MHT (Lemonnier *et al.* 1999). For such a depth extent, the observed Bouguer anomaly requires a density of 2590–2610 kg m^{-3}, which falls in the range of typical values for granites.

It thus turns out that density contrasts between the Lower Siwaliks, Middle Siwaliks, Lesser Himalayan meta-sediments and the Palung granites are sufficient to account for most of the gravity anomalies that remain once the flexural support of the range is taken into account. At this point we have considered only the mechanical effect of the thermal structure of the crust, and neglected the petrological structure that might result from the pressure and temperature conditions.

4 DENSITY CONTRASTS EXPECTED FROM THE PETROLOGICAL STRUCTURE

We now assess the effect of the petrological transformations that might occur during advection of the rocks through the steady-state temperature and pressure fields computed in Section 3. We analyse the petrological structure in terms of density variations and compare the expected gravity anomalies with observations.

4.1 Description of the thermal model

Because the approximation used in Section 3 to compute the temperature field in the underthrusting Indian plate might not be valid for computing the temperature field in the whole Himalayan crustal wedge, for this section the thermal structure was determined on the basis of a 2-D finite-element model described in more detail by Henry *et al.* (1997). It assumes a prescribed kinematics of thrust faulting consistent with the observed slip rate on the MHT (Lavé & Avouac 2000) and with the measured geodetic displacements (Larson *et al.* 1999). Erosion in the high range is assumed to balance tectonic uplift exactly. Shear heating on the MHT, mantle heat flow, and upper crustal radioactivity are also accounted for. The assumed boundary conditions are a constant surface temperature of 0 °C and a bottom heat flow of 15 mW m^{-2}. The temperature field (Fig. 7a) is computed with a radioactive heat production in the upper crust of 2.5 μW m^{-3}.

4.2 Effect of deep petrological transformations

Assuming instantaneous metamorphic transformations in response to *in situ* (P, T) conditions, Henry *et al.* (1997) determined equilibrium densities of crustal rocks within the Himalaya. Metamorphic facies and associated densities are obtained from a simplified petrogenetic grid (Bousquet *et al.* 1997). In this model, thermal expansion is taken into account using a constant thermal expansion coefficient $\alpha = 24 \times 10^{-6}\,K^{-1}$ (Turcotte & Schubert 1982). Actually, thermal expansion depends on temperature and on the rock mineral composition. In

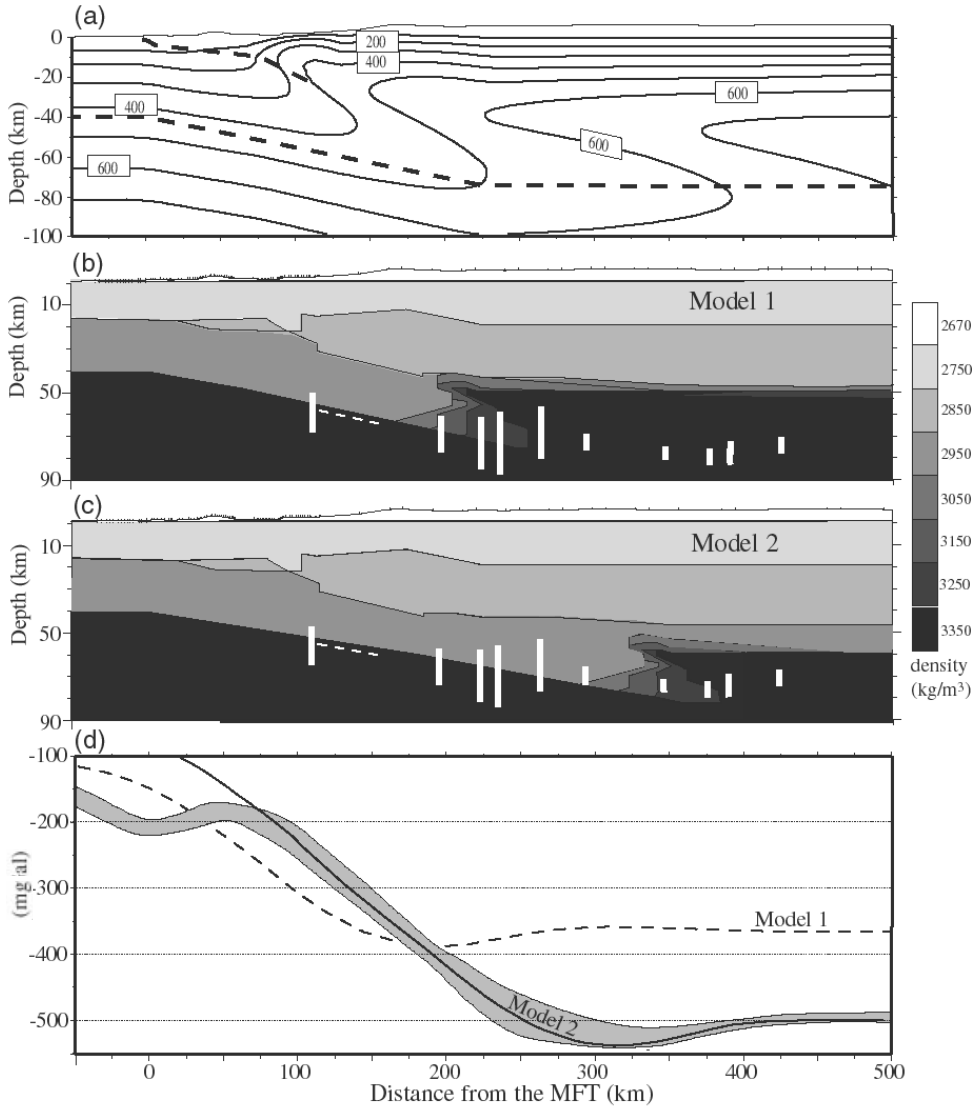

Figure 7. (a) Steady-state temperature field derived from a 2-D computation in which the kinematics of thrust faulting and erosion at the surface is prescribed (after Henry *et al.* 1997). (b) Density model deduced from a steady-state thermo-petrological model showing eclogitization of the lower crust beneath the Himalayan range (modified from Henry *et al.* 1997). White lines show constraints on Moho depths derived from INDEPTH (dashed line from seismic profile and vertical bars from receiver functions). The Bouguer anomaly (dashed line in d) associated with the density model in (b) is found to be inconsistent with the data (grey shading in d), by as much as 150 mgal under Tibet. It therefore suggests that eclogitization does not occur as south as shown in (b). The dashed curve in (d) exhibits a warped anomaly (km 100 to 250) with wavelength and amplitude strikingly comparable with those observed in the data north of the high range (km 200 to 350). (c) Modified model assuming that eclogitization is delayed by 6.5–8.5 Myr, possibly due to the kinetics of petrological changes. The corresponding anomaly (black line in d) is much more consistent with the gravity data.

Appendix A, in order to estimate the maximum influence of the thermal expansion, we have recomputed the gravity effect of this thermal expansion term when crustal rocks are given a granite-type thermal expansion coefficient. Though of second order, this effect is found to be non-negligible, reaching 80 mgal under southern Tibet.

The effect of increased pressure at depth is also corrected for: bulk moduli for the crust and for the mantle are computed assuming a constant Poisson's ratio $\nu_{crust} = \nu_{mantle} = 0.25$, and two Young's moduli namely $E_{crust} = 90$ GPa and $E_{mantle} = 175$ GPa associated with the crust and mantle, respectively. In this model, eclogitization of the lower crust occurs immediately north of the Higher Himalaya, where temperatures of about 500–550 °C are reached, and produces an increase in density of about $+300$ kg m^{-3} at depths between 55 and 75 km (Fig. 7b). The resulting Bouguer anomaly (dashed line in Fig. 7d) is clearly inconsistent with the data by as much as 150 mgal under Tibet. Note that this model does not fit the Moho depths determined from the receiver functions in southern Tibet either (Fig. 7b). Therefore, we conclude that complete eclogitization of the lower crust is certainly not occurring beneath the Himalaya of Nepal. However, a striking implication of this model is that it produces a Bouguer anomaly with a sharp hinge followed to the north by a positive upwarp (km 100 to 250 along the dashed line in Fig. 7d). This gravity oscillation mimics the one observed in the data but appears to be offset to the south by about 130 km. This feature may therefore be taken to suggest that some eclogitization would occur farther north than expected from the assumption of instantaneous petrological changes, possibly due to some delay induced by the kinetics of

petrological changes. Assuming a 15–20 mm yr^{-1} underthrusting rate, a 6.5–8.5 Myr delay time would then be necessary to account for the 130 km horizontal shift. The corresponding density model is shown in Fig. 7(c), with the associated gravity signature in Fig. 7(d) (solid line). The joint horizontal and vertical shift of the Indian crust along the MHT decollement results in a remarkably good fit to the Bouguer anomaly. The 6.5–8.5 Myr delay might be due to low water availability, which has proved to be a critical factor in metamorphic processes occurring in the lower crust (e.g. Austrheim 1990; Rubie 1990). Henry *et al.* (1997) have shown that, although the *P–T–t* path followed by the Indian lower crust probably crosses the blueschist stability field, transformation into blueshist facies rocks does not occur, probably because the 3–6 per cent water content necessary for the blueschist transformation is not available. Although the water content of lower crustal rocks equilibrated in the eclogite facies is only 0.4–1 per cent (Bousquet *et al.* 1997), transformation into eclogite may be delayed as long as free water is absent.

5 CONCLUSIONS

The main trend in the gravity data across the Himalaya reflects the deepening of the Moho from about 40 km beneath India to 75 km beneath Tibet, with a locally steeper Moho dip under the front of the high range. The gravity, together with seismological constraints on Moho depths, is correctly adjusted from a model in which the Indian lithosphere is flexed down gradually during underthrusting. The model, based on a realistic elastic–brittle–ductile rheology of the lithosphere, accounts for flexural and thermal weakening and therefore predicts a northward decrease of the EET. The shallow dip of the Moho and Indian basement in the foreland must result from a relatively high flexural rigidity of the Indian lithosphere, corresponding to a EET of 40–50 km. According to our model it requires a relatively strong lower crust, with diabase-like rheology, to minimize decoupling effects. Northwards, strain weakening of the lithosphere occurs, as it is flexed down under the load of topography and heated by the deep rocks brought up along the MHT. This allows the observed steep gravity gradient beneath the high range to be correctly accounted for.

At short wavelengths (20–50 km), density contrasts of probable lithological origin, especially at the MFT and the MBT, are shown to account for most of the gravity signal. At intermediate wavelengths, the negative hinge and positive upwarp observed in the gravity data under southern Tibet suggest a more complex loading of the underthrusting Indian plate or density distribution than assumed in our model. This feature might be explained by advocating additional bending moments (Lyon-Caen & Molnar 1983, 1985; Jin *et al.* 1996) or buckling of the mantle lid (Jin *et al.* 1994). We here suggest that this feature may result from density contrasts in the underthrusted Indian crust due to petrological transformations. Data exclude instantaneous equilibrium eclogitization of the Indian lower crust (Henry *et al.* 1997), but we find that the gravity data can be adjusted to allow for an about 130 km northward shift of the zone of eclogitization. Such a shift might result from delayed eclogitization possibly due to low water availability in the lower crust. This model is essentially a geometrical one and cannot be used to invalidate or to confirm elastic models that require bending moment (Lyon-Caen & Molnar 1983, 1985; Jin *et al.* 1996) from a subducting Indian slab. Actually, our model is compatible with a subduction of both Indian lithosphere and eclogitized lowermost crust beneath Tibet (Kosarev *et al.* 1999).

ACKNOWLEDGMENTS

This paper has greatly benefited from thoughtful reviews by S. L. Klemperer and E. B. Burov, who raised several important questions and contributed significantly to the clarity of the paper. This study was funded by the IDYL program (CNRS/INSU) and by CEA. Mr Pandey, Tandukar and Bashyal of the Nepalese Department of Mines and Geology are thanked for their help in organizing the field survey. We are also grateful to Mr Timilsina and Chaudhary from PEPP and Mr Nilgobinda from the Nepalese Geodetic Survey, for their help in the field.

REFERENCES

Abtout, A., 1987. La détermination des anomalies des champs de potentiel (magnétisme, gravimétrie) et la structure de la lithosphère continentale en Asie, *Thèse de 3ième cycle,* Université Paris VII, Paris.

Austrheim, H., 1990. The granulite-eclogite facies transition, a comparison of experimental work and natural occurrence in the Bergen arc, western Norway, *Lithos,* **25,** 163–169.

Bousquet, R., Goffé, B., Henry, P., Le Pichon, X. & Chopin, C., 1997. Kinematic, thermal and petrological model of the Central Alps: Lepontine metamorphism in the upper crust and eclogitisation in the lower crust, *Tectonophysics,* **273,** 105–127.

Brown, L.D., Zhao, W., Nelson, K.D., Hauck, M., Alsdorf, D., Ross, A., Cogan, M., Clark, M., Liu, X. & Che, J., 1996. INDEPTH deep seismic reflection observation of a regionally extensive high-amplitude basement reflector, and associated 'bright spots' beneath the northern Yadong-Gulu rift, Tibet, *Science,* **274,** 1688–1690.

Burov, E.B. & Diament, M., 1992. Flexure of the continental lithosphere with multilayered rheology, *Geophys. J. Int.,* **109,** 449–468.

Burov, E.B. & Diament, M., 1995. The effective elastic thickness (T_e) of continental lithosphere: What does it really mean?, *J. geophys. Res.,* **100,** 3905–3927.

Burov, E.B. & Diament, M., 1996. Isostasy, effective elastic thickness (*EET*) and inelastic rheology of continents and oceans, *Geology,* **24,** 419–422.

Carter, N.L. & Tsenn, M.C., 1987. Flow properties of continental lithosphere, *Tectonophysics,* **136,** 27–63.

Cattin, R. & Avouac, J.P., 2000. Modeling mountain building and the seismic cycle in the Himalaya of Nepal, *J. geophys. Res.,* **105,** 13 389–13 407.

Chayé d'Albissin, M. & Sirieys, P., 1989. Thermal deformability of rocks: relation to rock structure, in *Rock at Great Depth,* pp. 363–370, eds Maury, V. & Fourmaintraux, D., A. A. Balkema, Rotterdam.

Das, D., Mehra, G., Rao, K.G.C., Roy, A.L. & Narayana, M.S., 1979. Bouguer, free-air and magnetic anomalies over northwestern Himalaya, Himalayan Geology seminar, Section III, Oil and Natural Gas Resources, *Geol. Surv. India Misc. Publ.,* **41,** 141–148.

Forsberg, R., 1985. Gravity field terrain effect computations by FFT, *Bull. Géod.,* **59,** 342–360.

Gansser, A., 1981. The geodynamic history of the Himalaya, in *Zagros, Hindu Kush, Himalaya, Geodynamic Evolution,* pp. 111–121, eds Gupta, H. & Delany, F., Am. geophys. Un., Washington D.C.

Hassani, R., Jongmans, D. & Chéry, J., 1997. Study of plate deformation and stress in subduction processes using two-dimensional numerical models, *J. geophys. Res.,* **102,** 17 951–17 965.

Henry, P., Le Pichon, X. & Goffé, B., 1997. Kinematic, thermal and petrological model of the Himalaya: constraints related to metamorphism within the underthrust Indian crust and topographic elevation, *Tectonophysics,* **273,** 31–56.

Hirn, A., Sapin, M., Lépine, J.C., Xu, Z.X., Gao, E.Y., Teng, J.W. & Pandey, M.R., 1984. Crustal structure and variability of the Himalayan border of Tibet, *Nature,* **307,** 23–25.

Jeanloz, R. & Knittle, E., 1986. *Chemistry and Physics of Terrestrial Planets,* pp. 275–309, Springer Verlag, New York.

Jin, Y., McNutt, K. & Zhu, Y., 1994. Evidence from gravity and topography data for folding of Tibet, *Nature,* **371,** 669–674.

Jin, Y., McNutt, M.K. & Zhu, Y.S., 1996. Mapping the descent of Indian and Eurasian plates beneath the Tibetan Plateau from gravity anomalies, *J. geophys. Res.,* **101,** 11 275–11 290.

Kind, R., Ni, J., Zhao, W., Wu, J., Yuan, X., Zhao, L., Sandvol, E., Reese, C., Nabelek, J. & Hearn, T., 1996. Mid-crustal low-velocity zone beneath the southern Lhasa block: Results from the INDEPTH-II earthquake recording program, *Science,* **274,** 1692–1694.

Kirby, S.H. & Kronenberg, A.K., 1987. Rheology of the lithosphere: selected topics, *Rev. Geophys.,* **25,** 1219–1244.

Kono, M., 1974. Gravity anomalies in East Nepal and their implications to the crustal structure of the Himalaya, *Geophys. J. R. astr. Soc.,* **39,** 283–299.

Kosarev, G., Kind, R., Sobolev, S.V., Yuan, X., Hanka, W. & Oreshin, S., 1999. Seismic evidence for a detached Indian lithospheric mantle beneath Tibet, *Science,* **283,** 1306–1309.

Larson, K., Bürgmann, R., Bilham, R. & Freymueller, J.T., 1999. Kinematics of the India-Eurasia collision zone from GPS measurements, *J. geophys. Res.,* **104,** 1077–1093.

Lavé, J. & Avouac, J.P., 2000. Active folding and abandoned fluvial terraces across the Siwalik hills (Nepal), *J. geophys. Res.,* **105,** 5735–5770.

Le Pichon, X., Henry, P. & Goffé, B., 1997. Uplift of Tibet: from eclogites to granulites—implications for the Andean plateau and the Variscan belt, *Tectonophysics,* **273,** 57–76.

Lemonnier, C., Marquis, G., Perrier, F., Avouac, J.P., Chitrakar, G., Kafle, B., Sapkota, S., Gautam, U., Tiwari, D. & Bano, M., 1999. Electrical structure of the Himalaya of Central Nepal: high conductivity around the mid-crustal ramp along the MHT, *Geophys. Res. Lett.,* **26,** 3261–3264.

Lyon-Caen, H. & Molnar, P., 1983. Constraints on the structure of the Himalaya from an analysis of gravity anomalies and a flexural model of the lithosphere, *J. geophys. Res.,* **88,** 8171–8191.

Lyon-Caen, H. & Molnar, P., 1985. Gravity anomalies, flexure of the Indian plate and the structure, support and evolution of the Himalaya and Ganga Basin, *Tectonics,* **4,** 513–538.

McKenzie, D. & Fairhead, D., 1997. Estimates of effective elastic thickness of the continental lithosphere from Bouguer and gravity anomalies, *J. geophys. Res.,* **102,** 27 523–27 552.

Martelet, G., Sailhac, P., Moreau, F. & Diament, M., 2001. Characterization of geological boundaries using 1-D wavelet transform on gravity data; theory and application to the Himalayas, *Geophysics,* **66,** 1116–1129.

Métivier, F., Gaudemer, Y., Tapponnier, P. & Klein, M., 1999. Mass accumulation rates in Asia during the Cenozoic, *Geophys. J. Int.,* **137,** 280–318.

Nelson, K.D. *et al.*, 1996. Partially molten middle crust beneath Southern Tibet, synthesis of project INDEPTH results, *Science,* **274,** 1684–1688.

Pandey, O.P. & Agrawal, P.K., 1999. Lithospheric mantle deformation beneath the Indian cratons, *J. Geol.,* **107,** 683–692.

Ranalli, G., 1994. Nonlinear flexure and equivalent mechanical thickness of the lithosphere, *Tectonophysics,* **240,** 107–114.

Royden, L.H., 1993. The steady-state thermal structure of eroding orogenic belts and accretionary prisms, *J. geophys. Res.,* **98,** 4487–4507.

Rubie, D.C., 1990. Role of kinetics in the formation and preservation of eclogites, in *Eclogite Facies Rocks,* pp. 111–140, ed. Carswell, D.A., Blackie, Glasgow.

Saul, J., Kumar, N.R. & Sarkar, D., 2000. Lithospheric and upper mantle structure of the Indian Shield, from teleseismic receiver functions, *Geophys. Res. Lett.,* **27,** 2357–2360.

Schelling, D. & Arita, K., 1991. Thrusts tectonics, crustal shortening and the structure of the Far Eastern Nepal Himalaya, *Tectonics,* **10,** 851–862.

Sun, W., 1989. *Bouguer Gravity Anomaly Map of the People's Republic of China,* Chin. Acad. Geoexplor., Beijing.

Tsenn, M.C. & Carter, N.L., 1987. Upper limits of power-law creep of rocks, *Tectonophysics,* **136,** 1–26.

Turcotte, D.L. & Schubert, G., 1982. *Geodynamics: Application of Continuum Physics to Geological Problems,* John Wiley and Sons, New York.

Van de Meulebrouck, J., 1983. Reconnaissance geophysique des structures crustales de deux segments de chaîne de collision: le Haut Allier (Massif Central français) et le Sud Tibet (Himalaya), *Thèse de 3ième cycle,* Université des Sciences et Techniques du Languedoc, Montpellier.

Woollard, G.P. & Godley, V.M., 1980. *The New Gravity System: Changes in the International Gravity Base Values and Anomaly Values,* University of Hawaii, Honolulu.

Zhao, W., Nelson, K.D. & project INDEPTH Team, 1993. Deep seismic-reflection evidence of continental underthrusting beneath southern Tibet, *Nature,* **366,** 557–559.

APPENDIX A: ESTIMATION OF THE GRAVITY EFFECT OF THE THERMAL EXPANSION OF ROCKS

Owing to the thermal expansion of rocks, a temperature increase at depth induces density variations such that

$$\frac{\Delta\rho}{\rho} = -\alpha(T)\Delta T + \frac{1}{K}\Delta P, \tag{A1}$$

where ρ is the density, T the temperature, α the thermal expansion coefficient, K the bulk modulus, and P the lithostatic pressure. In orogenic belts such as the Himalaya, where the crust is particularly thick, the high temperatures at depth may

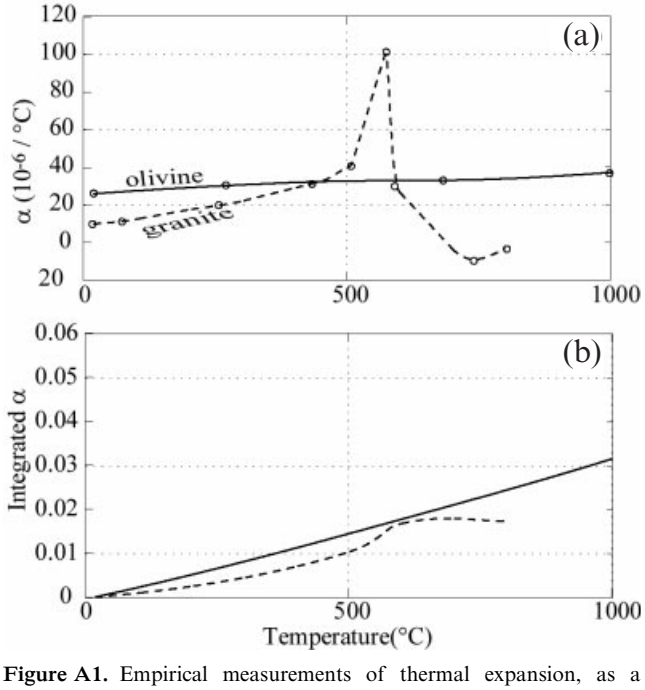

Figure A1. Empirical measurements of thermal expansion, as a function of temperature, for granite (Jeanloz & Knittle 1986) and olivine (Chayé d'Albissin & Sirieys 1989). (b) Temperature-integrated form of the thermal expansion coefficients in (a).

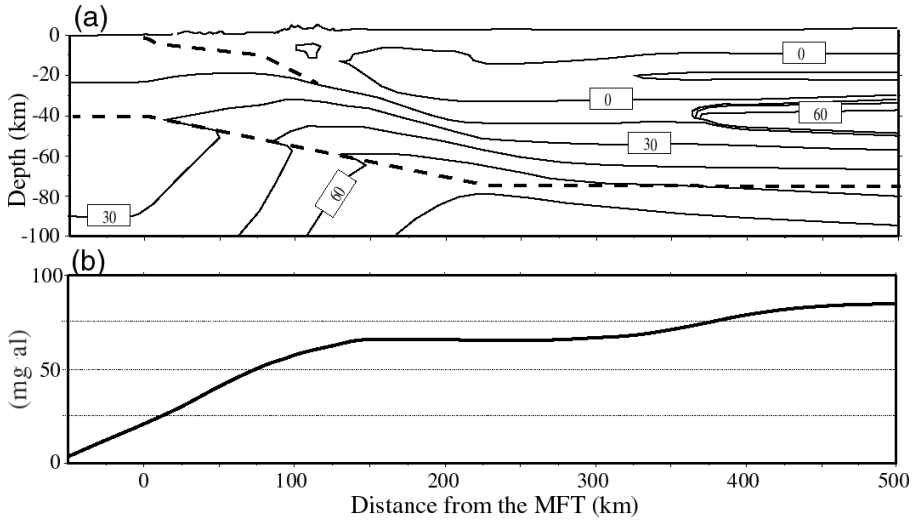

Figure A2. (a) Density variations resulting from thermal expansion and bulk modulus of rocks (isovalues in kg m^{-3}). This computation corresponds to the end-member case when crustal rocks are given a granite-type thermal expansion coefficient (see Appendix A). (b) Gravity corrections implied by (a) are as high as 80 mgal under southern Tibet.

be related to noticeable gravity variations. In fact, the thermal expansion of a rock $\alpha(T)$, depends on several parameters such as its granularity, heterogeneity, or water content, but is mostly sensitive to its mineral composition. In particular, the presence of quartz is crucial due to a particularly high thermal expansion at temperatures around 500–550 °C. In order to estimate some upper bound of the gravity signature, we have assumed a quartz-rich crustal composition and used an empirical law determined from the thermal expansion of granite (Chayé d'Albissin & Sirieys 1989).

For mantle rocks we use an empirical law determined from the thermal expansion of olivine (Jeanloz & Knittle 1986) (Fig. A1). Since α is a function of T, the density variations are determined through integration of eq. (A1) over the temperature range. The resulting density variations and the associated gravity effect are plotted in Figs A2 (a) and (b), respectively. The computed gravity effect reaches as much as 80 mgal beneath the Tibetan plateau. The rapid increase of α for temperatures close to 550 °C for granites (Fig. A1) plays an important role in the density variations induced by thermal expansion at the crustal scale.

As a conclusion, we see that, in the context of active orogenic belts, the thermal expansion effect induced by the thickening of the crust can reach several tens of milligals.